Letter

Generalized cross-resonance scheme for maximally entangling two-qutrit gates

Yash Saxena [1,2,*] Tharrmashastha SAPV [2,3,†] Sagnik Chatterjee [2,3,4,‡] and Ray-Kuang Lee [1,5,6,§]

[1] *Department of Physics, National Tsing Hua University, Hsinchu City 300013, Taiwan*
[2] *Center for Quantum Technologies, IIIT-Delhi, New Delhi 110020, India*
[3] *Department of Computer Science, IIIT-Delhi, New Delhi 110020, India*
[4] *School of Technology and Computer Science, TIFR, Mumbai 400005, India*
[5] *Institute of Photonics Technologies, National Tsing Hua University, Hsinchu 30013, Taiwan*
[6] *Center for Quantum Science and Technology, Hsinchu 30013, Taiwan*

(Received 10 June 2025; accepted 25 June 2026; published 12 August 2026)

To utilize higher-dimensional quantum systems, in this Letter we derive a generalized cross-resonance scheme for realizing maximally entangling two-qutrit gates on fixed-frequency transmons beyond the 0–1 subspace. Our two-qutrit gates, namely, $\mathrm{U}_{\mathrm{CR}}^{01}$ and $\mathrm{U}_{\mathrm{CR}}^{12}$, acting on the 0–1 and 1–2 energy transitions of transmons, respectively, *directly* allow for entanglement on the 1–2 levels. Unlike the known works, our gate is parametric in nature, enabling us to construct multiple entangling gates of interest. By performing simulations in Qiskit, we demonstrate two-qutrit generalized controlled-X ($\mathrm{U}_{\mathrm{CX}}^{01}$ and $\mathrm{U}_{\mathrm{CX}}^{12}$) and controlled-$H$ ($\mathrm{U}_{\mathrm{CH}}^{01}$ and $\mathrm{U}_{\mathrm{CH}}^{12}$) gates, which are instances of the proposed U_{CR} gates, with reported gate fidelities of 93.17% (99.73%), 91.47% (97.88%), 96.06% (99.39%), and 95.68% (98.99%), respectively, with (and without) noise. We also reveal a two-qutrit Bell state with a fidelity of 87.54% (99.06%), with a complete Bell state preparation in an $\sim$514 ns pulse sequence, which is less than the gate time of the known scheme by cross-Kerr-based entangling gates.

DOI: 10.1103/qqtg-x6jg

Working with multilevel quantum systems instead of qubit systems offers many intrinsic advantages with respect to quantum computation and information. Access to larger Hilbert spaces has proved beneficial for a myriad of tasks such as qubit reset [1–3], qubit readout [4], fidelity in quantum teleportation [5,6], randomness generation [7], entanglement purification [8], construction of qudit quantum error-correcting codes [9–11], and to improve security, robustness, and enhance key rates for quantum key distribution (QKD) protocols [12–14]. Qudit systems have also been provably shown to exhibit speedup and separations in quantum circuit complexity compared to their classical counterparts [15,16]. More concretely, it has been observed that fewer qudit gates are required to implement a given unitary operation compared to the qubit case [17–20]. Three-level systems or *qutrits*, specifically, have been used to obtain sublinear depth decompositions of qubit circuits without ancilla [21,22]. This reduction in the depth leads to an improvement of the scalability of quantum circuits primarily by ensuring longer decoherence times [23,24].

Quantum devices consisting of mesoscopic anharmonic oscillators have emerged as the leading architecture in the race for realizing physical quantum systems over the last decade [25]. Circuit quantum electrodynamics (cQED) studies the interaction of anharmonic oscillators constructed from nonlinear superconducting circuit elements such as the Josephson junction, with quantized electromagnetic fields in the microwave-frequency domain [26,27]. The energy spectrum of cQED devices is governed by macroscopic circuit element parameters, which makes these devices highly configurable. Moreover, superconducting transmons demonstrate large nonlinearity [28–31], thereby allowing us to restrict the dynamics of the quantum system precisely to the number of levels we desire, making them particularly favorable for implementing qutrits and other higher-level systems.

Consequently, research intensity on extending cQED devices to three-level (and higher) systems has increased, resulting in a flurry of recent works focused on implementing qutrit-based quantum algorithms on superconducting transmons [32,33]. However, currently, in order to implement arbitrary qutrit-based quantum algorithms on superconducting qutrits, one needs to design building blocks specifically for transmons that allow us to implement a set of qutrit gates that is *universal* for three-level quantum computation. Exact universality on qutrits requires a discrete set of single-qutrit Hamiltonians and one two-qutrit Hamiltonian [34–36]. While high-fidelity single-qutrit quantum gates have long been realized [33,37–39], realizations of two-qutrit

[*] Contact author: ysaxena@gapp.nthu.edu.tw
[†] Contact author: tharrmashasthav@iiitd.ac.in
[‡] Contact author: sagnikc@iiitd.ac.in
[§] Contact author: rklee@ee.nthu.edu.tw

entangling gates using cross-resonance (CR) scheme either suffered from increased crosstalk or were limited to perform a direct entanglement on only the 0–1 subspace of the entire two-qutrit Hilbert space [40,41]. Researchers addressed these issues by realizing maximally entangling two-qutrit gates on the superconducting transmon architecture using differential ac Stark shift drives with nontunable and tunable couplings [42,43]. However, using small cross-Kerr coupling for entangling gates leads to slow gate operations.

In this Letter, we address the challenges posed due to entanglement confined to 0–1 subspace and slow gate times, by extending the well-established and faster cross-resonance scheme to a generalized qutrit architecture. For this, we theorize and demonstrate, via simulations, two-qutrit gates on fixed-frequency, fixed-coupling transmons that enable high-fidelity, maximally entangling operations across the entire two-qutrit space. This work provides a viable route toward universal qutrit-based quantum computation using experimentally accessible resources. Moving forward, we demonstrate two-qutrit generalized controlled-X and controlled-H gates, using the cross-resonance framework. The tunability required for effective interaction in the two transmon qutrits with fixed frequencies can be achieved using microwave pulse control [44–47]. Our simulation setup consists of fixed-frequency transmons (modeled as qutrits) coupled via a resonator. The individual frequencies of the two qutrits are $\omega_1/2\pi = 4.9$ GHz and $\omega_2/2\pi = 5.5$ GHz. The anharmonicities considered for the simulations are $\delta_1 = -400$ MHz and $\delta_2 = -300$ MHz. The qutrits interact with a coupling strength of $J/2\pi = 2.7$ MHz and are individually coupled to the resonator with coupling constants as $g_1/2\pi = 0.62$ GHz and $g_2/2\pi = 0.64$ GHz, respectively, ensuring reliable gate execution.

By performing simulations using Qiskit Dynamics, we realize high-fidelity two-qutrit generalized controlled-X and controlled-H gates, namely, U_{CX}^{01}, U_{CX}^{12}, U_{CH}^{01}, and U_{CH}^{12}, with and without decoherence noise. Furthermore, we prepare two-qutrit Bell states with fidelities of $99.06\% \pm 0.01\%$ and $87.54\% \pm 0.01\%$ in the noiseless and the noisy settings, respectively. Notably, the fidelity in the noiseless setting is comparable to the current state of the art, and has been achieved using a relatively simpler technique for the current superconducting quantum hardware.

Two-qutrit interactions for the realization of entangling gates are controllable entirely by microwave pulses, and this has been extensively experimentally demonstrated earlier [40,48]. Here, we employ simple amplitude modulation of Gaussian square pulses for two-qutrit operations, along with Gaussian pulses with quadrature derivative removal via adiabatic gate (DRAG) for single-qutrit operations. This activates our two-qutrit gate, which is fully characterized and utilized to generate maximally entangled states.

For superconducting architectures, one of the most prominent techniques to drive transmons is the CR technique [49,50]. This technique has been explored and studied for the experimental realization of high-fidelity two-qubit quantum gates, for instance, the controlled-NOT gate [51,52]. This amplitude-modulated microwave-only technique significantly reduces hardware complexity, as it allows control pulses to be delivered through the same lines used for sending standard single-qutrit control signals. Additionally, the cross-resonance gate offers a distinct approach to entangling operations by avoiding the need for frequency tuning or coupler modulation, typically required in other methods. Because it operates effectively with fixed-frequency transmon qutrits, the CR gate naturally avoids noise introduced by dynamic frequency adjustments. Transmon-based qutrits, known for their strong coherence properties (longer coherence times), low sensitivity to charge fluctuations, and high single-qutrit gate fidelities, are particularly compatible with this scheme. Hence, for large, fault-tolerant systems, the CR gate approach tends to be more robust and engineering-friendly. This has been the driving force for the cross-resonance gate to be widely adopted for implementing two-qutrit gates in superconducting architectures with fixed-frequency transmons [40].

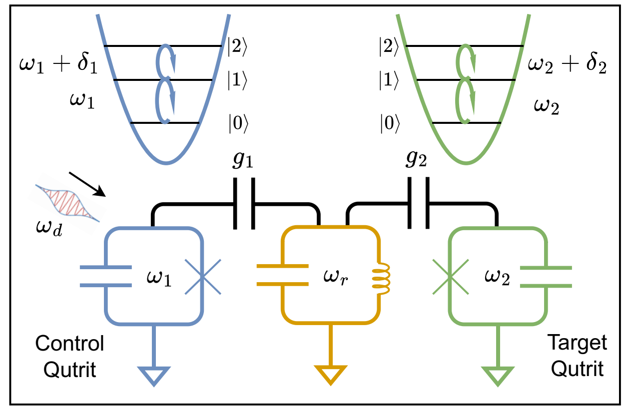

FIG. 1. The schematic diagram of a coupled two-transmon system. ω_1 and ω_2 correspond to the frequency of the transition $|0\rangle \to |1\rangle$ in transmon 1 and transmon 2, respectively, and δ_1 and δ_2 are their respective anharmonicities. The two transmons are coupled through a resonator of frequency ω_r with coupling strengths g_1 and g_2, respectively. The proposed generalized cross-resonance scheme generalizes the qubit-qubit cross-resonance scheme to the qutrit setting, where the control qutrit (transmon 1) is irradiated with a microwave pulse of frequency ω_d, which equals either ω_2 corresponding to $|0\rangle \to |1\rangle$ transition or $\omega_2 + \delta_2$ corresponding to $|1\rangle \to |2\rangle$ transition of the target qutrit (transmon 2).

In this interaction, a microwave pulse is applied to one transmon (the control) at the resonant frequency of the other (the target) (Fig. 1). The interplay between the inherent coupling and the applied drive generates Rabi oscillations in the target qutrit, where the state of the control qutrit determines the oscillation frequency of the target qutrit. This conditional interaction forms the basis of the CR gate, enabling high-fidelity entangling operations without requiring direct frequency tuning.

For two-level systems, the cross-resonance technique, for a particular drive power, results in two distinct Rabi frequencies, γ_0 and γ_1. The Hamiltonian for this interaction can be described as

$$H_{\mathrm{cr}}^{\mathrm{qubit}} = \gamma_0 |0\rangle\langle 0| \otimes \sigma_x + \gamma_1 |1\rangle\langle 1| \otimes \sigma_x, \quad (1)$$

where $\gamma_0 = w_1/2$ and $\gamma_1 = -w_1/2$, with w_1 being the $|0\rangle \to |1\rangle$ transition frequency of qubit 1.

Extending the idea of cross-resonance to a two-qutrit system, we show, in the Supplemental Material [53], that the effective drive Hamiltonian of a microwave pulse on one qutrit with frequency resonant to the other qutrit can be given as

$$\begin{aligned} H_{\rm CR}^{\rm qutrit}(t) = &\left(-\frac{J\Omega(t)}{4}\right)\left[\{\nu_0|0\rangle\langle 0| + \nu_1|1\rangle\langle 1| + \nu_2|2\rangle\langle 2|\}\right. \\ &\otimes \left\{\eta_{20}\left(e^{i(\omega_d-\omega_2^{01})t}|0\rangle\langle 1| + e^{-i(\omega_d-\omega_2^{01})t}|1\rangle\langle 0|\right)\right. \\ &+ \sqrt{2}\eta_{21}\left(e^{i(\omega_d-\omega_2^{12})t}|1\rangle\langle 2|\right. \\ &\left.\left.\left. + e^{-i(\omega_d-\omega_2^{12})t}|2\rangle\langle 1|\right)\right\}\right], \end{aligned} \tag{2}$$

where ω_d is the drive frequency and $\Omega(t)$ is the microwave-drive amplitude, along with $\omega_2^{01} = \omega_2$, $\omega_2^{12} = \omega_2 - \delta_2$, $\nu_0 = -\eta_{10}$, $\nu_1 = \eta_{10} - 2\eta_{11}$, and $\nu_2 = 2\eta_{11}$, with $\eta_{10} = 1/\omega_1$, $\eta_{11} = 1/(\omega_1 + \delta_1)$, $\eta_{20} = 1/\omega_2$, and $\eta_{21} = 1/(\omega_2 + \delta_2)$.

It is apparent from the expression of $H_{\rm CR}^{\rm qutrit}(t)$ that the excitations in the target qutrit occur on the 0–1 level if the drive frequency conforms to the $|0\rangle \to |1\rangle$ transition frequency of the target qutrit and occur on the 1–2 level if the drive frequency matches the $|1\rangle \to |2\rangle$ transition frequency. Depending on the choice of the drive frequency, this Hamiltonian gives rise to one of the two gates,

$$\begin{aligned} \mathrm{U}_{\rm CR}^{01}(\theta) &= \sum_{i=0}^{2} |i\rangle\langle i| \otimes R_X^{01}(\nu_i\theta) \\ &= |0\rangle\langle 0| \otimes e^{-i(|0\rangle\langle 1|+|1\rangle\langle 0|)\nu_0\theta} + |1\rangle\langle 1| \otimes \mathbb{I} \\ &\quad + |2\rangle\langle 2| \otimes e^{-i(|0\rangle\langle 1|+|1\rangle\langle 0|)\nu_2\theta} \end{aligned} \tag{3}$$

or

$$\begin{aligned} \mathrm{U}_{\rm CR}^{12}(\theta) &= \sum_{i=0}^{2} |i\rangle\langle i| \otimes R_X^{12}(\nu_i\theta) \\ &= |0\rangle\langle 0| \otimes e^{-i(|1\rangle\langle 2|+|2\rangle\langle 1|)\nu_0\theta} + |1\rangle\langle 1| \otimes \mathbb{I} \\ &\quad + |2\rangle\langle 2| \otimes e^{-i(|1\rangle\langle 2|+|2\rangle\langle 1|)\nu_2\theta}. \end{aligned} \tag{4}$$

Here, the rotations are $R_X^{01}(\nu_i\theta) = e^{-i(|0\rangle\langle 1|+|1\rangle\langle 0|)\nu_i\theta/2} \equiv RX^{01}(\phi_i)$ on 0–1 space, and, on 1–2 subspace, $R_X^{12}(\nu_i\theta) = e^{-i(|1\rangle\langle 2|+|2\rangle\langle 1|)\nu_i\theta/2} \equiv RX^{12}(\phi_i)$.

These gates can be seen as direct analogs of the two-qubit CR gate on the 0–1 and 1–2 transition levels, respectively. In addition, they generalize the gates of the prior works [40,48] that use the cross-resonance framework on just two of the three levels. Our work improves upon the prior works in two primary ways. First is the ability to perform a direct entanglement on the 1–2 levels of the target qutrit. While the previous works use the ability to entangle on 0–1 levels to perform entanglement on the 1–2 levels, our gates bring in the ability to perform entanglement directly on the 1–2 levels of the target qutrit. Second, $\mathrm{U}_{\rm CR}^{01}$ and $\mathrm{U}_{\rm CR}^{12}$ are not individual gates but rather a class of gates (i.e., they are parametric in nature) that directly allow entanglement on 0–1 and 1–2 levels and can be used to construct a multitude of entangling gates of interest. However, all gates proposed prior to this work are specific nonparametric gates. In addition to these contrasts, the action of $\mathrm{U}_{\rm CR}^{01}$ and $\mathrm{U}_{\rm CR}^{12}$ on the target qutrit uniquely depends on the state of the control qutrit, and no two states of control induce the same oscillation on the target qutrit. This is evident both in the simulation results [53] and in gate descriptions (3) and (4). Although these gates individually act on a two-level subspace of the three-level systems, together they span the complete two-qutrit Hilbert space.

To demonstrate this maximal spanning, we use the generalized CR to construct controlled-X and controlled-H gates on the 0–1 and 1–2 subspaces, which we define as

$$\begin{aligned} U_{\rm CX}^{01} = &|0\rangle\langle 0| \otimes \begin{bmatrix} 0 & 1 & 0 \\ 1 & 0 & 0 \\ 0 & 0 & i \end{bmatrix} + |1\rangle\langle 1| \otimes \begin{bmatrix} 1 & 0 & 0 \\ 0 & 1 & 0 \\ 0 & 0 & 1 \end{bmatrix} \\ &+ |2\rangle\langle 2| \otimes \begin{bmatrix} 0 & 1 & 0 \\ 1 & 0 & 0 \\ 0 & 0 & -i \end{bmatrix}, \end{aligned} \tag{5}$$

$$\begin{aligned} U_{\rm CX}^{12} = &|0\rangle\langle 0| \otimes \begin{bmatrix} i & 0 & 0 \\ 0 & 0 & 1 \\ 0 & 1 & 0 \end{bmatrix} + |1\rangle\langle 1| \otimes \begin{bmatrix} 1 & 0 & 0 \\ 0 & 1 & 0 \\ 0 & 0 & 1 \end{bmatrix} \\ &+ |2\rangle\langle 2| \otimes \begin{bmatrix} -i & 0 & 0 \\ 0 & 0 & 1 \\ 0 & 1 & 0 \end{bmatrix} \end{aligned} \tag{6}$$

and

$$\begin{aligned} U_{\rm CH}^{01} = &|0\rangle\langle 0| \otimes \frac{1}{\sqrt{2}}\begin{bmatrix} 1 & 1 & 0 \\ -1 & 1 & 0 \\ 0 & 0 & \sqrt{2} \end{bmatrix} + |1\rangle\langle 1| \\ &\otimes \begin{bmatrix} 1 & 0 & 0 \\ 0 & 1 & 0 \\ 0 & 0 & 1 \end{bmatrix} + |2\rangle\langle 2| \otimes \frac{1}{\sqrt{2}}\begin{bmatrix} 1 & -1 & 0 \\ 1 & 1 & 0 \\ 0 & 0 & \sqrt{2} \end{bmatrix}, \end{aligned} \tag{7}$$

$$\begin{aligned} U_{\rm CH}^{12} = &|0\rangle\langle 0| \otimes \frac{1}{\sqrt{2}}\begin{bmatrix} \sqrt{2} & 0 & 0 \\ 0 & 1 & 1 \\ 0 & -1 & 1 \end{bmatrix} + |1\rangle\langle 1| \\ &\otimes \begin{bmatrix} 1 & 0 & 0 \\ 0 & 1 & 0 \\ 0 & 0 & 1 \end{bmatrix} + |2\rangle\langle 2| \otimes \frac{1}{\sqrt{2}}\begin{bmatrix} \sqrt{2} & 0 & 0 \\ 0 & 1 & -1 \\ 0 & 1 & 1 \end{bmatrix}. \end{aligned} \tag{8}$$

We perform numerical simulations of the proposed gates using Qiskit Dynamics [54], both with and without the inclusion of decoherence effects. For effective decoherence time, we have considered amplitude damping (T_1: energy relaxation time) and phase damping (T_2: phase coherence time). We have also performed quantum process tomography (QPT) and studied the fidelities of our proposed gates with respect to varying decoherence times, and the results are presented in Sec. V of the Supplemental Material [53]. The noiseless simulations were performed by simulating the Hamiltonian dynamics, and the noisy simulations were performed by simulating the Lindbladian dynamics. The Lindblad operators corresponding to the qutrit amplitude and phase damping, which we have considered in this work, are presented in the Supplemental Material [53]. For the noisy simulations, we assume identical coherence times across both qutrits and set $T_1^{12} = T_1^{01}/2$ and $T_2^{12} = T_2^{01}/2$ to account for the reduced coherence of the $|1\rangle \leftrightarrow |2\rangle$ transition.

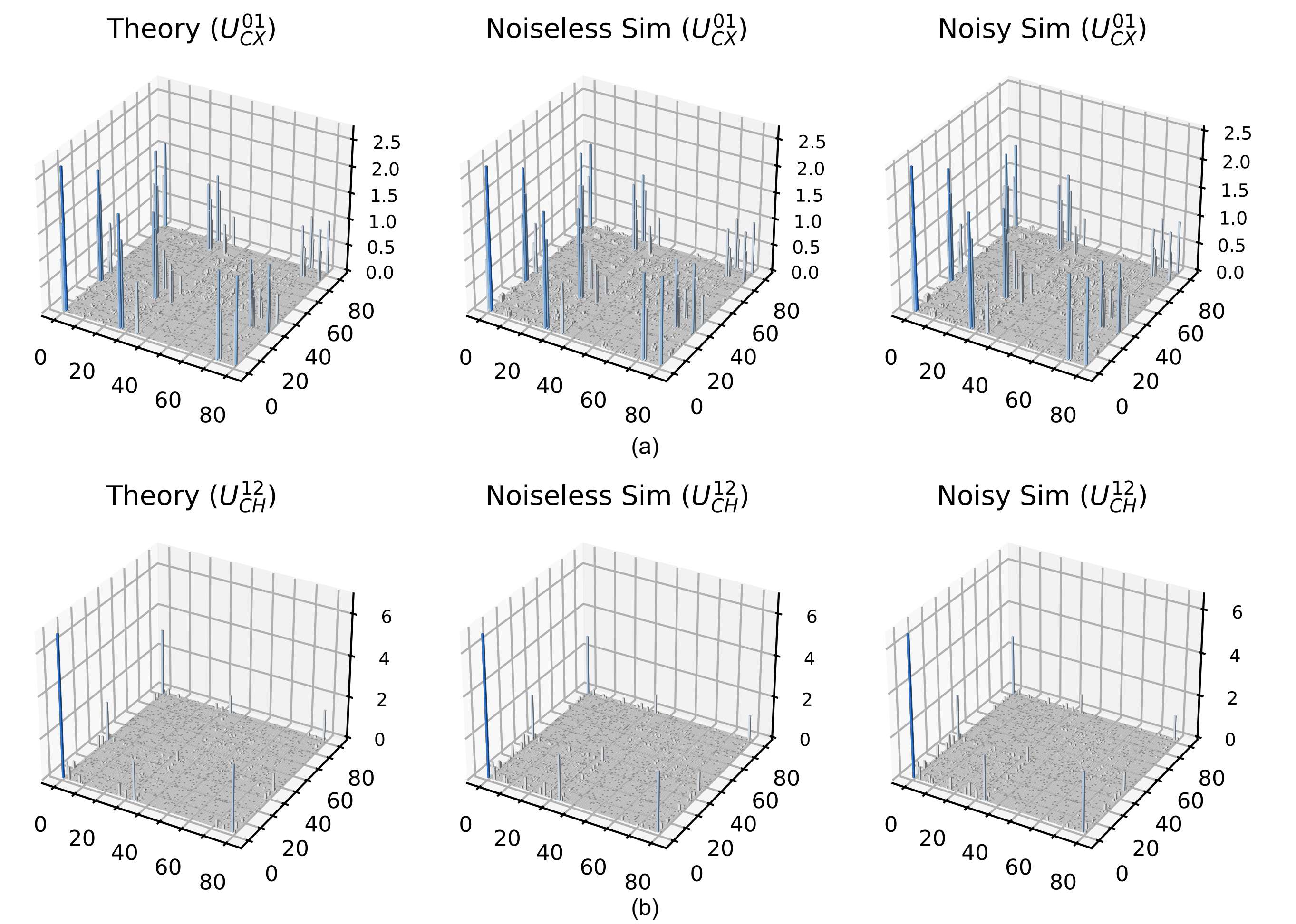

FIG. 2. The comparison between the process matrices χ_{ideal}, $\chi_{\text{noiseless}}$, and χ_{noisy} of the ideal gates and the gates simulated without and with the effects of decoherence. (a) The process matrices of the $\mathrm{U}_{\mathrm{CX}}^{01}$ gate obtained using QPT. We obtain process fidelities of $99.73\% \pm 0.01\%$ and $93.17\% \pm 0.01\%$ for the simulated $\mathrm{U}_{\mathrm{CX}}^{01}$ gate without and with decoherence noise, where the decoherence time T $(T_1 = T_2 = T) = 2500\,\mu\text{s}$. (b) The process matrices of the $\mathrm{U}_{\mathrm{CH}}^{12}$ gate obtained using QPT. We obtain process fidelities of $98.99\% \pm 0.01\%$ and $95.68\% \pm 0.01\%$ for the simulated $\mathrm{U}_{\mathrm{CH}}^{12}$ gate without and with decoherence noise, where the decoherence time T $(T_1 = T_2 = T) = 2500\,\mu\text{s}$.

Using QPT (Fig. 2), we obtain the process fidelities ($\mathcal{F}$) of these gates. Without decoherence effects, we obtain $\mathcal{F}(\mathrm{U}_{\mathrm{CX}}^{01}) = 99.73\% \pm 0.01\%$, $\mathcal{F}(\mathrm{U}_{\mathrm{CX}}^{12}) = 97.88\% \pm 0.01\%$, $\mathcal{F}(\mathrm{U}_{\mathrm{CH}}^{01}) = 99.39\% \pm 0.01\%$, and $\mathcal{F}(\mathrm{U}_{\mathrm{CH}}^{12}) = 98.99\% \pm 0.01\%$. Under the effects of decoherence, where $T_1 = T_2 = 2500\,\mu\text{s}$, we obtain fidelities of $\mathcal{F}(\mathrm{U}_{\mathrm{CX}}^{01}) = 93.17\% \pm 0.01\%$, $\mathcal{F}(\mathrm{U}_{\mathrm{CX}}^{12}) = 91.47\% \pm 0.01\%$, $\mathcal{F}(\mathrm{U}_{\mathrm{CH}}^{01}) = 96.06\% \pm 0.01\%$, and $\mathcal{F}(\mathrm{U}_{\mathrm{CH}}^{12}) = 95.68\% \pm 0.01\%$. For comparison, we also obtain the process fidelities of identity gates of lengths 200 and 100 ns (gate times of U_{CX} and U_{CH}, respectively) under the same noise parameters, and we obtain $\mathcal{F}(\mathbb{I}_{200}) = 93.80\% \pm 0.01\%$ and $\mathcal{F}(\mathbb{I}_{100}) = 97.10\% \pm 0.01\%$. Note that these fidelities are very close to the U_{CX} and U_{CH} gates, respectively.

Further, we use $\mathrm{U}_{\mathrm{CX}}^{01}$ and $\mathrm{U}_{\mathrm{CH}}^{12}$ gates, along with single-qutrit gates, to demonstrate that the proposed generalized CR gates span the complete two-qutrit Hilbert space by preparing the two-qutrit Bell state:

$$|\psi\rangle = \frac{1}{\sqrt{3}}(|00\rangle + |11\rangle + |22\rangle). \tag{9}$$

The exact pulse sequence of the Bell state preparation circuit can be found in the Supplemental Material [53].

The parameters used for the simulations mimic those of the actual backend, which were provided earlier. For the two-qutrit Bell state preparation, we use quantum state tomography (QST) to reconstruct the prepared states (Fig. 3) and observe fidelities of $\mathcal{F}_{\text{noiseless}} = 99.06\% \pm 0.01\%$ without decoherence and $\mathcal{F}_{\text{noisy}} = 87.54\% \pm 0.01\%$ with decoherence, where $T_1 = T_2 = 2500\,\mu\text{s}$. For our simulator parameters, we obtain the total gate time corresponding to the Bell state preparation circuit as $\sim$514 ns.

In conclusion, we extend the qubit cross-resonance scheme to qutrit systems and show that it allows spanning the entire two-qutrit Hilbert space and achieving maximal entanglement. To advocate this, we construct two-qutrit gates, namely, $\mathrm{U}_{\mathrm{CX}}^{01}$, $\mathrm{U}_{\mathrm{CX}}^{12}$, $\mathrm{U}_{\mathrm{CH}}^{01}$, and $\mathrm{U}_{\mathrm{CH}}^{12}$, and use them with single-qutrit gates to prepare a high-fidelity two-qutrit Bell state. While previous works on the cross-resonance scheme for qutrits were limited to just two of the three dimensions of the qutrit Hilbert space [40,48], our work improves upon them to show the possibility of exploring the complete qutrit Hilbert space

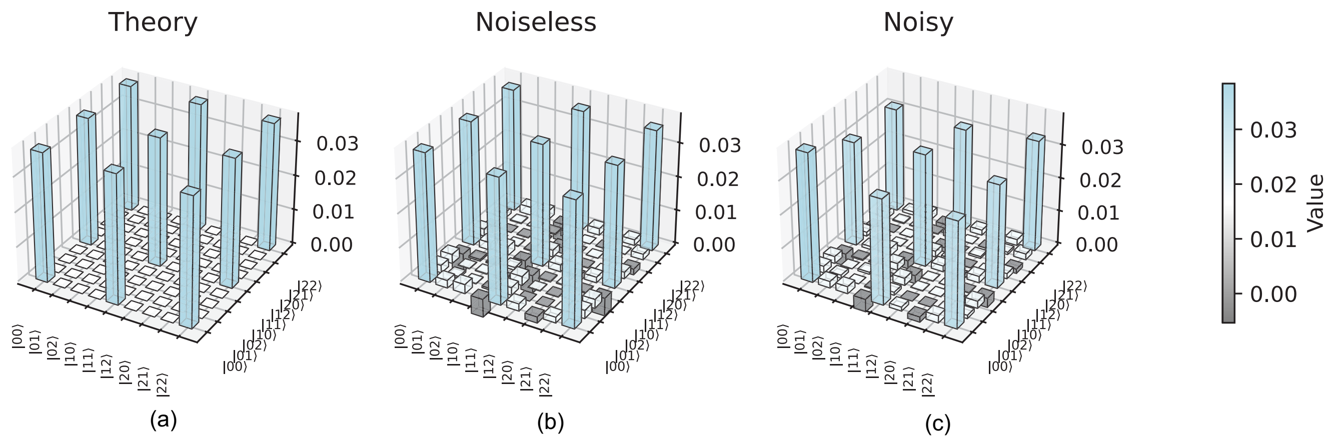

FIG. 3. The QST plots of (a) the two-qutrit Bell state as defined in Eq. (9), (b) the two-qutrit Bell state prepared under the noiseless setting, and (c) the two-qutrit Bell state prepared under the noisy setting ($T_1 = T_2 = 2500\,\mu\mathrm{s}$). We prepare the two-qutrit Bell state using the proposed $\mathrm{U}_{\mathrm{CX}}^{01}$ and $\mathrm{U}_{\mathrm{CH}}^{12}$ gates and obtain state fidelities of $\mathcal{F}_{\text{noiseless}} = 99.06\% \pm 0.01\%$ and $\mathcal{F}_{\text{noisy}} = 87.54\% \pm 0.01\%$, respectively. For our choice of parameters, the total time for the preparation of the qutrit Bell state is $\sim$514 ns.

using cross-resonance. Our technique of extending and generalizing the cross-resonance scheme also outperforms the modified cross-Kerr techniques of prior works in terms of gate times [42,43].

We further notice that, for our parameters of the simulation, we achieve a Bell state preparation time that is significantly lower than those due to prior works. This work throws light on one of the central concerns of gate timings that is posed on the CR scheme and shows the possibility of spanning much larger Hilbert spaces using considerably less gate times by generalizing the CR technique. This eliminates the need to invoke and work with more complex approaches for the current hardware architectures.

A possible interesting direction of future work is to investigate whether we can obtain a maximally entangling gate on $d > 2$ level systems using a single pulse. Further, while our work focuses on fixed-frequency transmon qutrits, recent advances in fluxonium qubit platforms [55–57] present interesting opportunities for future extension of generalized cross-resonance scheme. Another interesting direction for future work is the development of scalable frequency-allocation and collision-avoidance strategies for multiqutrit architectures, where frequency crowding arising from both the 0–1 and 1–2 transitions poses additional challenges beyond those encountered in qubit-based processors. These investigations could be of paramount importance for the field of superconducting quantum computation and information processing on higher-level systems, specifically qutrits.

Y.S. and R.-K.L. were partially supported by the National Science and Technology Council of Taiwan (No. 114-2112-007-044-MY3, No. 114-26229-007-005, No. 115-2119-M-008-001, and No. 115-2923-M-007-001-MY3). Y.S., T.S., and S.C. would like to acknowledge the constant support that we received from Dr. Debajyoti Bera. S.C. and T.S. would also like to thank Harsh Rathee and Ming-Tso W. for extensive discussions on qutrits. Y.S. would also like to thank the Center for Quantum Technologies (CQT), IIIT-Delhi, India, for funding support in the initial phase of this work. The work of S.C. was partially supported by the Department of Atomic Energy, Government of India, under Project No. RTI4014.

Data availability. The data supporting this study's findings are available within the article [61].

[1] D. Basilewitsch, J. Fischer, D. M. Reich, D. Sugny, and C. P. Koch, Fundamental bounds on qubit reset, Phys. Rev. Res. **3**, 013110 (2021).

[2] C. M. Diniz, R. J. de Assis, N. G. de Almeida, and C. J. Villas-Boas, Optimizing resetting of superconducting qubits, Phys. Rev. A **108**, 052605 (2023).

[3] D. J. Egger, M. Werninghaus, M. Ganzhorn, G. Salis, A. Fuhrer, P. Müller, and S. Filipp, Pulsed reset protocol for fixed-frequency superconducting qubits, Phys. Rev. Appl. **10**, 044030 (2018).

[4] P. Jurcevic, A. Javadi-Abhari, L. S. Bishop, I. Lauer, D. F. Bogorin, M. Brink, L. Capelluto, O. Günlük, T. Itoko, N. Kanazawa *et al.*, Demonstration of quantum volume 64 on a superconducting quantum computing system, Quantum Sci. Technol. **6**, 025020 (2021).

[5] S. Roy, S. Mal, and A. Sen(De), Gain in performance of teleportation with uniformity-breaking distributions, Phys. Rev. A **105**, 022610 (2022).

[6] A. Fonseca, High-dimensional quantum teleportation under noisy environments, Phys. Rev. A **100**, 062311 (2019).

[7] P. Skrzypczyk and D. Cavalcanti, Maximal randomness generation from steering inequality violations using qudits, Phys. Rev. Lett. **120**, 260401 (2018).

[8] J. Miguel-Ramiro and W. Dür, Efficient entanglement purification protocols for d-level systems, Phys. Rev. A **98**, 042309 (2018).

[9] P. J. Nadkarni and S. S. Garani, Quantum error correction architecture for qudit stabilizer codes, Phys. Rev. A **103**, 042420 (2021).

[10] R. F. Uy and D. A. Gangloff, Qudit-based quantum error-correcting codes from irreducible representations of SU(d), Phys. Rev. A **112**, 042402 (2025).
[11] A. Tanggara, M. Gu, and K. Bharti, Simple construction of qudit Floquet codes on a family of lattices, arXiv:2410.02022.
[12] T. Durt, D. Kaszlikowski, J.-L. Chen, and L. C. Kwek, Security of quantum key distributions with entangled qudits, Phys. Rev. A **69**, 032313 (2004).
[13] S. P. Walborn, D. S. Lemelle, M. P. Almeida, and P. H. Souto Ribeiro, Quantum key distribution with higher-order alphabets using spatially encoded qudits, Phys. Rev. Lett. **96**, 090501 (2006).
[14] T. Durt, N. J. Cerf, N. Gisin, and M. Żukowski, Security of quantum key distribution with entangled qutrits, Phys. Rev. A **67**, 012311 (2003).
[15] A. B. Grilo, E. Kashefi, D. Markham, and M. de Oliveira, The power of shallow-depth Toffoli and qudit quantum circuits, ACM (2026), doi: 10.1145/3802819.
[16] M. de Oliveira, S. Subramanian, L. Mendes, and M.-H. Hsieh, Unconditional advantage of noisy qudit quantum circuits over biased threshold circuits in constant depth, Nat. Commun. **16**, 3559 (2025).
[17] A. Muthukrishnan and C. R. Stroud, Quantum fast Fourier transform using multilevel atoms, J. Mod. Opt. **49**, 2115 (2002).
[18] T. C. Ralph, K. J. Resch, and A. Gilchrist, Efficient Toffoli gates using qudits, Phys. Rev. A **75**, 022313 (2007).
[19] A. Pavlidis and E. Floratos, Quantum-Fourier-transform-based quantum arithmetic with qudits, Phys. Rev. A **103**, 032417 (2021).
[20] G. Agrawal, T. K. Konar, L. G. C. Lakkaraju, and A. Sen(De), Tradeoff between noise and banding in a quantum adder with qudits, Phys. Rev. A **111**, 032408 (2025).
[21] P. Gokhale, J. M. Baker, C. Duckering, N. C. Brown, K. R. Brown, and F. T. Chong, Asymptotic improvements to quantum circuits via qutrits, in *Proceedings of the 46th International Symposium on Computer Architecture*, ISCA '19 (Association for Computing Machinery, New York, 2019), pp. 554–566.
[22] J. M. Baker, C. Duckering, P. Gokhale, N. C. Brown, K. R. Brown, and F. T. Chong, Improved quantum circuits via intermediate qutrits, ACM Trans. Quantum Comput. **1**, 1 (2020).
[23] Y. Wang, Z. Hu, B. C. Sanders, and S. Kais, Qudits and high-dimensional quantum computing, Front. Phys. **8**, 589504 (2020).
[24] H. Miyahara, Y. Chen, V. Roychowdhury, and L.-S. Bouchard, Decoherence mitigation by embedding a logical qubit in a qudit, Quantum Inf. Proc. **22**, 278 (2023).
[25] F. Arute, K. Arya, R. Babbush, D. Bacon, J. C. Bardin, R. Barends, R. Biswas, S. Boixo, F. G. Brandao, D. A. Buell *et al.*, Quantum supremacy using a programmable superconducting processor, Nature (London) **574**, 505 (2019).
[26] A. Blais, R.-S. Huang, A. Wallraff, S. M. Girvin, and R. J. Schoelkopf, Cavity quantum electrodynamics for superconducting electrical circuits: An architecture for quantum computation, Phys. Rev. A **69**, 062320 (2004).
[27] A. Blais, A. L. Grimsmo, S. M. Girvin, and A. Wallraff, Circuit quantum electrodynamics, Rev. Mod. Phys. **93**, 025005 (2021).
[28] J. M. Fink, M. Göppl, M. Baur, R. Bianchetti, P. J. Leek, A. Blais, and A. Wallraff, Climbing the Jaynes–Cummings ladder and observing its nonlinearity in a cavity QED system, Nature (London) **454**, 315 (2008).
[29] I. Schuster, A. Kubanek, A. Fuhrmanek, T. Puppe, P. W. H. Pinkse, K. Murr, and G. Rempe, Nonlinear spectroscopy of photons bound to one atom, Nat. Phys. **4**, 382 (2008).
[30] L. S. Bishop, J. M. Chow, J. Koch, A. A. Houck, M. H. Devoret, E. Thuneberg, S. M. Girvin, and R. J. Schoelkopf, Nonlinear response of the vacuum Rabi resonance, Nat. Phys. **5**, 105 (2009).
[31] M. D. Reed, L. DiCarlo, B. R. Johnson, L. Sun, D. I. Schuster, L. Frunzio, and R. J. Schoelkopf, High-fidelity readout in circuit quantum electrodynamics using the Jaynes-Cummings nonlinearity, Phys. Rev. Lett. **105**, 173601 (2010).
[32] T. Roy, Z. Li, E. Kapit, and D. I. Schuster, Two-qutrit quantum algorithms on a programmable superconducting processor, Phys. Rev. Appl. **19**, 064024 (2023).
[33] P. Liu, R. Wang, J.-N. Zhang, Y. Zhang, X. Cai, H. Xu, Z. Li, J. Han, X. Li, G. Xue, W. Liu, L. You, Y. Jin, and H. Yu, Performing SU(d) operations and rudimentary algorithms in a superconducting transmon qudit for $d = 3$ and $d = 4$, Phys. Rev. X **13**, 021028 (2023).
[34] A. Y. Vlasov, Noncommutative tori and universal sets of nonbinary quantum gates, J. Math. Phys. **43**, 2959 (2002).
[35] R. Brylinski and G. Chen, *Mathematics of Quantum Computation*, *Computational Mathematics* (CRC Press, Boca Raton, FL, 2002).
[36] G. K. Brennen, D. P. O'Leary, and S. S. Bullock, Criteria for exact qudit universality, Phys. Rev. A **71**, 052318 (2005).
[37] M. A. Yurtalan, J. Shi, M. Kononenko, A. Lupascu, and S. Ashhab, Implementation of a Walsh-Hadamard gate in a superconducting qutrit, Phys. Rev. Lett. **125**, 180504 (2020).
[38] A. Morvan, V. V. Ramasesh, M. S. Blok, J. M. Kreikebaum, K. O'Brien, L. Chen, B. K. Mitchell, R. K. Naik, D. I. Santiago, and I. Siddiqi, Qutrit randomized benchmarking, Phys. Rev. Lett. **126**, 210504 (2021).
[39] M. Kononenko, M. A. Yurtalan, S. Ren, J. Shi, S. Ashhab, and A. Lupascu, Characterization of control in a superconducting qutrit using randomized benchmarking, Phys. Rev. Res. **3**, L042007 (2021).
[40] M. S. Blok, V. V. Ramasesh, T. Schuster, K. O'Brien, J. M. Kreikebaum, D. Dahlen, A. Morvan, B. Yoshida, N. Y. Yao, and I. Siddiqi, Quantum information scrambling on a superconducting qutrit processor, Phys. Rev. X **11**, 021010 (2021).
[41] L. E. Fischer, A. Chiesa, F. Tacchino, D. J. Egger, S. Carretta, and I. Tavernelli, Universal qudit gate synthesis for transmons, PRX Quantum **4**, 030327 (2023).
[42] N. Goss, A. Morvan, B. Marinelli, B. K. Mitchell, L. B. Nguyen, R. K. Naik, L. Chen, C. Jünger, J. M. Kreikebaum, D. I. Santiago, J. J. Wallman, and I. Siddiqi, High-fidelity qutrit entangling gates for superconducting circuits, Nat. Commun. **13**, 7481 (2022).
[43] K. Luo, W. Huang, Z. Tao, L. Zhang, Y. Zhou, J. Chu, W. Liu, B. Wang, J. Cui, S. Liu, F. Yan, M.-H. Yung, Y. Chen, T. Yan, and D. Yu, Experimental realization of two qutrits gate with tunable coupling in superconducting circuits, Phys. Rev. Lett. **130**, 030603 (2023).
[44] P. C. de Groot, J. Lisenfeld, R. Schouten, S. Ashhab, A. Lupaşcu, C. Harmans, and J. Mooij, Selective darkening of degenerate transitions demonstrated with two superconducting quantum bits, Nat. Phys. **6**, 763 (2010).

[45] P. J. Leek, S. Filipp, P. Maurer, M. Baur, R. Bianchetti, J. M. Fink, M. Göppl, L. Steffen, and A. Wallraff, Using sideband transitions for two-qubit operations in superconducting circuits, Phys. Rev. B **79**, 180511(R) (2009).

[46] T. Yamamoto, Y. A. Pashkin, O. Astafiev, Y. Nakamura, and J. S. Tsai, Demonstration of conditional gate operation using superconducting charge qubits, Nature (London) **425**, 941 (2003).

[47] J. M. Chow, L. DiCarlo, J. M. Gambetta, F. Motzoi, L. Frunzio, S. M. Girvin, and R. J. Schoelkopf, Optimized driving of superconducting artificial atoms for improved single-qubit gates, Phys. Rev. A **82**, 040305(R) (2010).

[48] A. Cervera-Lierta, M. Krenn, A. Aspuru-Guzik, and A. Galda, Experimental high-dimensional Greenberger-Horne-Zeilinger entanglement with superconducting transmon qutrits, Phys. Rev. Appl. **17**, 024062 (2022).

[49] C. Rigetti and M. Devoret, Fully microwave-tunable universal gates in superconducting qubits with linear couplings and fixed transition frequencies, Phys. Rev. B **81**, 134507 (2010).

[50] J. M. Chow, A. D. Córcoles, J. M. Gambetta, C. Rigetti, B. R. Johnson, J. A. Smolin, J. R. Rozen, G. A. Keefe, M. B. Rothwell, M. B. Ketchen, and M. Steffen, Simple all-microwave entangling gate for fixed-frequency superconducting qubits, Phys. Rev. Lett. **107**, 080502 (2011).

[51] S. Sheldon, E. Magesan, J. M. Chow, and J. M. Gambetta, Procedure for systematically tuning up cross-talk in the cross-resonance gate, Phys. Rev. A **93**, 060302(R) (2016).

[52] A. Kandala, A. Mezzacapo, K. Temme, M. Takita, M. Brink, J. M. Chow, and J. M. Gambetta, Hardware-efficient variational quantum eigensolver for small molecules and quantum magnets, Nature (London) **549**, 242 (2017).

[53] See Supplemental Material at http://link.aps.org/supplemental/10.1103/qqtg-x6jg for detailed derivations of the effective Hamiltonian, quantum process tomography, Bell-state preparation, Lindblad jump operators, leakage analysis, and additional simulation results, which includes Refs. [58–60].

[54] D. Puzzuoli, C. J. Wood, D. J. Egger, B. Rosand, and K. Ueda, Qiskit dynamics: A Python package for simulating the time dynamics of quantum systems, J. Open Source Software **8**, 5853 (2023).

[55] M. Hita-Pérez, P. A. Orellana, J. J. García-Ripoll, and M. Pino, Bound states in the continuum in a fluxonium qutrit, Phys. Rev. A **106**, 062602 (2022).

[56] W. Ardati, S. Léger, S. Kumar, V. N. Suresh, D. Nicolas, C. Mori, F. D'Esposito, T. Vakhtel, O. Buisson, Q. Ficheux, and N. Roch, Using bifluxon tunneling to protect the fluxonium qubit, Phys. Rev. X **14**, 041014 (2024).

[57] R. A. Mencia, W.-J. Lin, H. Cho, M. G. Vavilov, and V. E. Manucharyan, Integer fluxonium qubit, PRX Quantum **5**, 040318 (2024).

[58] P. Krantz, M. Kjaergaard, F. Yan, T. P. Orlando, S. Gustavsson, and W. D. Oliver, A quantum engineer's guide to superconducting qubits, Appl. Phys. Rev. **6**, 021318 (2019).

[59] S. Richer, Perturbative analysis of two-qubit gates on transmon qubits, Master's thesis, JARA Institute for Quantum Information, RWTH Aachen University, Aachen, Germany, 2013.

[60] M. A. Nielsen and I. L. Chuang, *Quantum Computation and Quantum Information: 10th Anniversary Edition* (Cambridge University Press, Cambridge, 2010).

[61] Y. Saxena, T. SAPV, S. Chatterjee, and R.-K. Lee, Maximally-Entangling-Two-Qutrit-CR, 2025, https://github.com/braqiiit/Maximally-Entangling-Two-Qutrit-CR.